Creep fracture mechanism of polycrystalline Ni-based superalloy with diffusion coatings

Kang Yuan[1, *], Ru Lin Peng[1], Xin-Hai Li[2], Lennart Johansson[2], Sten Johansson[1], Yan-dong Wang[3]

[1]Department of Management and Engineering, Linkoeping University, SE-58183 Linköping, Sweden

[2]Siemens Industrial Turbomachinery AB, SE-61283 Finspång, Sweden

[3]Beijing Institute of Technology, Beijing 100081, China

[*]Corresponding author: kang.yuan@liu.se

Abstract: Diffusion coatings are widely used to increase oxidation and corrosion resistance of hot superalloy components for gas turbines. The aim of this study is to investigate the effect of coatings (NiAl and PtAl) on the creep fracture mechanism of samples with a substrate of IN792. The samples have been creep tested at two temperatures (850 °C and 950 °C) and different applied tensile stresses, until failure between 205 and 21000 hrs. The observation of cross-sections by SEM shows that the microstructural evolution in the coating is dependent on the diffusion of alloying elements in the sample. Furthermore the time and temperature induced growth of the coating is found to be controlled only by inward diffusion of Al. Grain-boundary cracking is the basic fracture mode in the substrate in all samples irrespective if the crack is initiated from coating or substrate. The analysis of microstructure shows that the diffusion coatings display two types of mechanical behavior - being easily plasticized or cracked - dependent on temperature and type of coating, and therefore can be considered as non-load carrying regions. After recalculating the creep stress to exclude the final effective coating thickness from the total sample thickness, the coated samples showed similar creep rupture behavior as the uncoated samples in the Larson-Miller diagram.

Keywords: Creep; Ni-based superalloy; Diffusion coating; Crack

1. Introduction

Due to their excellent high-temperature mechanical properties, superalloys are widely used as base material for components in advanced gas turbine operating at high temperatures [1]. Components with Al-rich coatings become much even more sustainable with better resistance against environmental attack from high-temperature oxidation and corrosion. Aluminide diffusion coatings are widely used to protect the superalloys in a gas turbine at temperatures lower than 1000 °C [2]. Due to the difference of mechanical properties compared to the base material, the effect of coatings on the mechanical behavior of the substrate needs to be considered. At higher temperatures creep of the material become an important issue. There have been some investigations on creep mechanism of superalloys with high temperature coatings, which suggest several effects of coatings: a change in microstructure of the base material; a change of load distribution; introduction of cracks [3,4]. Some valuable creep tests (generally < 1000 hrs) of diffusion coating-superalloy system have been made during the past decades [5-8]. However long-term creep test results (> 1000 hrs) are seldom presented in the best literature surveys. Furthermore in some specific situations, the coating has to be deposited onto the thin part of the component, which makes the effect of coating more critical. The industrial background to this research work actually emanates from problems in the walls of the cooling channels which can be as thin as in the order of millimeters. The aim of this paper is to investigate the mechanical effect of diffusion coatings on thin sectioned superalloy specimens (~ 1 mm) subjected to creep at the operating temperatures.

2. Experimental procedures

Creep samples in the form of sheet were produced from cast of nickel based polycrystalline superalloy Inconel 792 (IN792) with the nominal chemical composition of Ni-12.5Cr-9Co-4.175W-4.175Ta-3.975Ti-3.375Al-1.9Mo-0.08C-0.0175Zr-0.015B (wt.%). A drawing of the specimens is shown in Fig. 1. Two kinds of diffusion coatings - NiAl and PtAl - were deposited onto the specimen surface by the CVD process at 1050-1100 °C for 12-20 hrs. The specimens were solution treated at 1120 °C for 2 hrs and then aged at 845 °C for 24 hrs, followed by air cooling to room temperature. The main phases in the alloy are a solid solution of nickel based γ (disordered FCC) and an intermetallic γ' (FCC_$L1_2$). Four types of specimens were used in this study (Table 1). Specimens coated with only NiAl or PtAl, and specimens coated with NiAl on one side but PtAl on the other including an uncoated reference. The creep samples were tested under different static tensile loads at 850 °C or 950 °C in air until failure. The tested samples were cut as cross sections in their longitudinal direction (loading direction) and then carefully ground and mechanically polished pre, to study the microstructure below the fracture surface. The microscopic characterization was carried out by using a *FEG-SEM Hitachi SU-70* scanning electron microscope (SEM) with an INCA *Oxford Instruments* energy dispersive system (EDS).

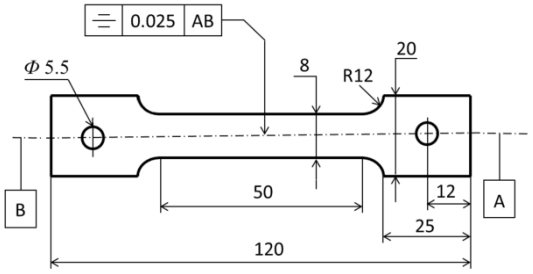

Figure 1. Dimensions of the sheet specimens with thickness of 1 mm (in millimeters).

Table 1. Sample type definition.

Sample type	Coating covering	
	One side	Another side
Uncoated	uncoated	uncoated
NiAl-NiAl	NiAl	NiAl
PtAl-PtAl	PtAl	PtAl
NiAl-PtAl	NiAl	PtAl

3. Results and discussion

3.1. Creep test and *effective coating thickness* (*ECT*)

Results from the creep tests are presented as applied stress versus creep life (Fig. 2). The creep lifetime varied largely between 205 hrs and 21000 hrs, depending on the testing temperature and applied stress. As expected, the resistances to creep rupture decreases with increasing test temperature, showing either a shorter creep life under the same applied stress or a lower applied stress for the same creep life. While the PtAl-PtAl at 850 °C shows scattered results and the

NiAl-PtAl has only two data points, a linear relationship between the applied stress and creep life, both plotted in logarithm scale, could be found for the other coated samples.

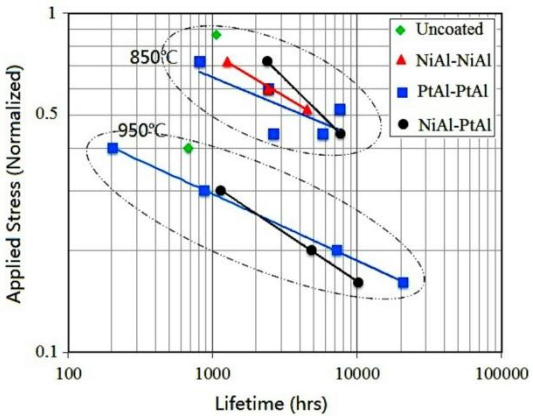

Figure 2. Creep lifetimes of specimens under different applied stresses (normalized) at 850 °C and 950 °C.

Based on their distinctive metallographic features, three characteristic zones are defined for the coatings (Fig. 3): outer zone (OZ), interdiffusion zone (IDZ) and second reactive zone (SRZ). The matrix phases in OZ, IDZ, SRZ and the substrate are respectively β, γ' (or β), γ' and γ. After long creep time at 900 °C the OZ shrinked in NiAl (Fig. 3(a)) but was well stabilized in PtAl (Fig. 3(b)), which indicates that Pt can restrict the β-to-γ' transformation by blocking the outward diffusion of Ti, Co, W and Ta. The enrichment of Cr, Mo and Co in those zones was responsible for the formation of some specific precipitates (i.e. TCP, Cr-α) which were observed in both NiAl and PtAl coatings. The phase identification in this research is achieved by comparing the EDS-detected composition with those given in literatures [1,9-11]. A more detailed analysis of the microstructural changes in the PtAl-PtAl samples could be found in [12].

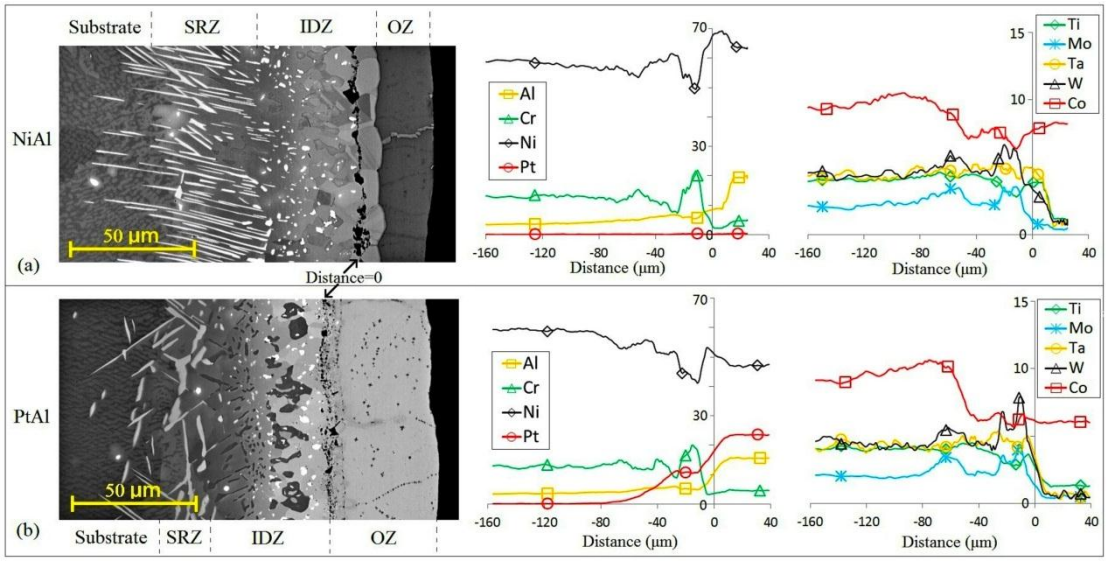

Figure 3. Microstructure and composition profiles (averaged from three different areas) on (a) NiAl side and (b) PtAl side in a NiAl-PtAl sample after creep test at 950 °C with lifetime 10244 hrs.

The micro-hardness tests of cross sections at room temperature show a variation along the diffusion coatings (Fig. 4(a)), verifying the difference in mechanical properties between coating and substrate. This means that the stress partitioning needs to be recalculated by considering the newly developed coating thickness. To encompass the growth of coating due to the diffusion of alloying elements

during the creep test an *effective coating thickness* (*ECT*) is defined, which is the total thickness of OZ, IDZ and SRZ. The inward diffusion of Al in the substrate is pre-assumed to control the movement of coating-substrate interface in both NiAl and PtAl coatings. The statistic results of the *ECT* in Fig. 4 (b) presents a linear correlation with $\sqrt{D^{Al} \times t}$, showing as

$$ECT = ECT_0 + C \times \sqrt{D^{Al} \times t} \quad (1)$$

In Eq. (1) ECT_0 is the original *effective coating thickness* and *C* is a constant. D^{Al} is the diffusion coefficient of Al in the substrate (IN792), calculated by using lower Hashin-Shrtikman bound [13]:

$$D^{Al} = D_{\gamma'}^{Al} + \frac{f_{\gamma}}{1/(D_{\gamma}^{Al} - D_{\gamma'}^{Al}) + f_{\gamma'}/(3D_{\gamma'}^{Al})} \quad (2)$$

In Eq. (2) D_{γ}^{Al} and $D_{\gamma'}^{Al}$ are the diffusion coefficient of Al in γ and γ' phases, f_{γ} and $f_{\gamma'}$ are the volume fraction of γ and γ' phases. The values of D_{γ}^{Al}, $D_{\gamma'}^{Al}$, f_{γ} and $f_{\gamma'}$ (listed in Fig. 4(b)) can be calculated by the software DICTRA [14] with Ni-based thermodynamic and kinetic database – TCNI5 and MOBNI2 [15]. The lower Hashin-Shrtikman bound [13] claims the easier-diffusion (high diffusivity) phase as the matrix phase which is likely the case in IN792 with the solid solution γ as the easier-diffusion and matrix phase. Actually applying another Hashin-Shrtikman bound (i.e. upper bound), which assumes the tougher-diffusion (lower diffusivity) phase as the matrix phase, gives the similar calculated results on diffusivity of Al in IN792 [12]. The paralleled curves in Fig. 4(b) give a coating-independent constant *C* (~ 2.54×10^5) in Eq. (1) for both NiAl and PtAl diffusion coatings, indicating that the coating thickening rate is controlled only by Al inward diffusion in the substrate. However this conclusion needs to be further checked since the statistic data scattering still exists in Fig. 4(b), especially when the $\sqrt{D^{Al} \times t}$ value is lower.

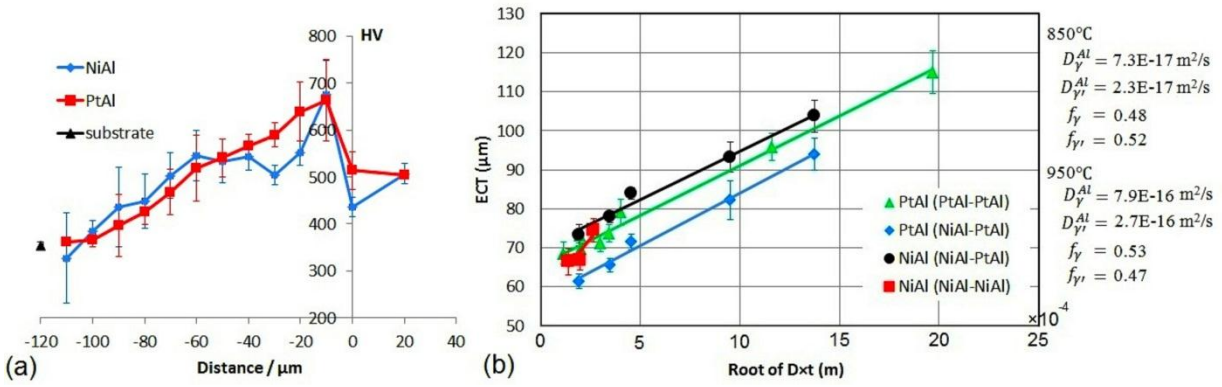

Figure 4. (a) Micro-hardness profiles (Vickers) in NiAl and PtAl measured at room temperature (in the same sample in Fig. 3) and (b) *Effective Coating Thickness* (*ECT*) near fracture surface vs. $\sqrt{D^{Al} \times t}$. The standard deviations (error bar) in both graphs are given by measurement at ~10 regions of the sample.

3.2. Morphology study of creep fracture

Because of heavy oxidation of the fracture surface fractographic analyses cannot be easily applied to study the creep rupture process. Instead, detailed microstructural examinations were carried out on polished lengthwise cross-sections cutting through the mid-width of the creep fractured specimens. The loading direction is in the length direction of the sample and is vertical in all the micrographs shown in this section.

3.2.1. Uncoated

Grain-boundary weakening is generally responsible for the creep failure of polycrystalline materials [16]. In the hot combustion and turbine sections of gas turbine the coarse-grained or even single-crystalline superalloys are commonly used to minimize the effect of grain boundary on creep behavior [1]. For polycrystalline superalloys (e.g. IN792) the addition of few ppm carbon, by forming carbides along grain boundaries, can improve the resistance of grain-boundary sliding [17]. Carbides detached from grain boundary of the superalloy by tensile force were observed by [18,19], which were also observed in the current study in the serrated crack path (Fig. 5(a)). According to the composition measurement by EDS two types of carbides were detected: (Cr,W)-rich $M_{23}C_6$ and (Ti,Ta)-rich MC. $M_{23}C_6$ was only observed along grain boundaries while MC was common both along grain boundaries and inside of the grains. The same microstructures have been reported in IN792 by other researchers [6,20]. The direction of the alignment of cracks is unsurprisingly perpendicular or near-perpendicular to the creep loading direction.

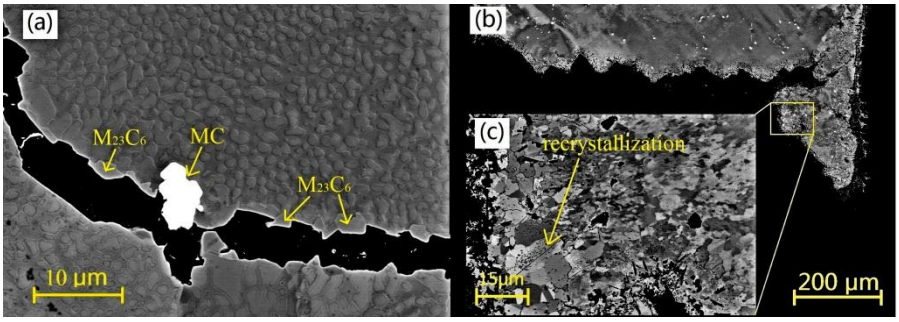

Figure 5. Fractured uncoated sample for 950 °C: (a) serrated grain-boundary crack with carbides, (b) morphology near fracture surface and (c) recrystallization near fracture surface.

The creep tests were conducted in air; consequently oxidation occurred at the sample' surface whether it was covered by coating or not. It has been reported that the surface oxide layer could lower the steady creep strain rate comparing with vacuum creep test (without surface oxidation) [21]. In this study oxidation was also present inside of material when the crack initiated from the surface. However such oxidation was reported to have little effect on the steady creep rate of the sample [6,20]. Fig. 5(b) shows the length-sectional morphology near the fracture surface of the uncoated sample. Since the crack propagates along the grain boundary, the roughness of the fracture surface is grain-size dependent. The appearance of recrystallization along the fracture surface indicates dynamic recrystallization caused by local plastic deformation during crack propagation at the creep testing temperature (Fig. 5(c)). Actually such recrystallization was also commonly observed along the fracture surface in other sample types.

3.2.2. NiAl-NiAl

Ductile-brittle transition temperature (DBTT) reflects the ductility of materials at high temperatures. The definition of DBTT is mainly based upon the amount of plastic deformation during failure. For instance Lowrie et al. [6,20] suggested the temperature above which the fracture strain of the

material was more than 0.6%. The coating can be even super-plastic at high enough temperature [22]. The DBTT of NiAl is 693 °C measured by [23]), which however should also be dependent upon the coating thickness according to the results of [24]. In this type of sample through-coating cracks were commonly found with the oxidation around (Fig. 6(a) and (b)). The formation of γ' in OZ may weaken the strength grain boundary and induce cracks (Fig. 6(c)). When a through-coating crack was meeting or is located near a grain boundary in the substrate, it could continue to penetrate into the substrate, being identified by the "L"-shape crack path near the coating part (Fig. 6(b)). The cracking of the coating makes it a non-load carrying member and leaves the substrate in a somewhat similar creep situation as the uncoated sample.

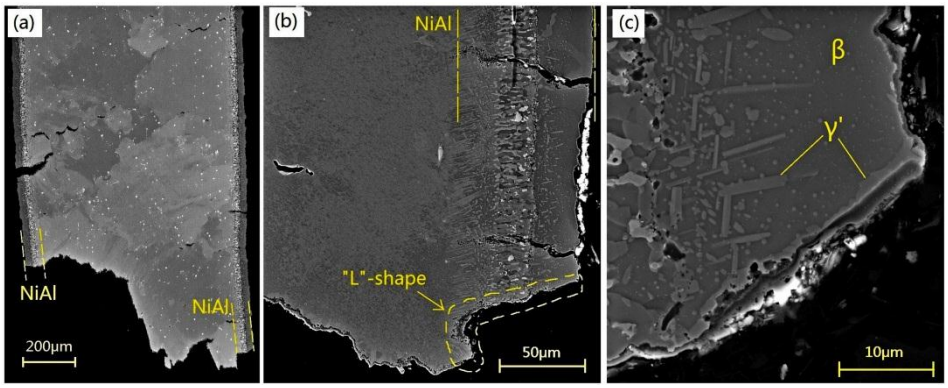

Figure 6. Fractured NiAl-NiAl sample for 850 °C: (a) morphology containing fracture surface, (b) "L"-shape path of though-coating cracks and (c) γ' precipitates in OZ. (The coating part is marked in Fig. 6-8).

3.2.3. PtAl-PtAl

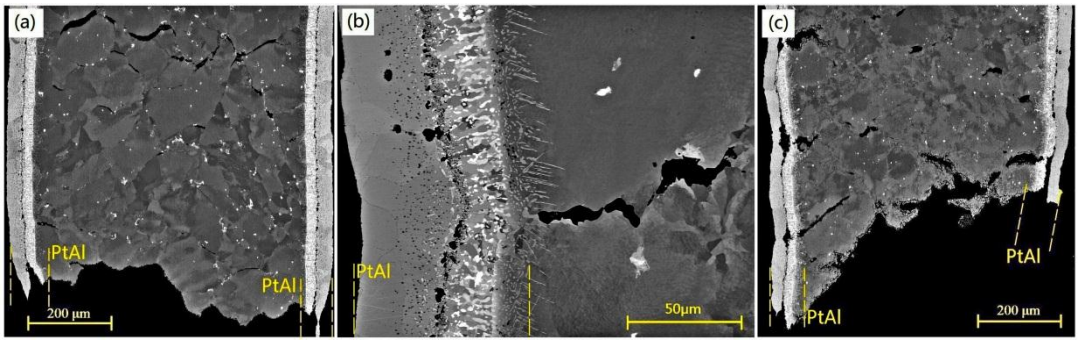

Figure 7. Fractured PtAl-PtAl sample: (a) morphology containing fracture surface (850 °C), (b) crack beneath PtAl (850 °C) and (c) morphology containing fracture surface (950 °C).

The addition of Pt into aluminide diffusion coating was initially intended to slow down the inward diffusion of Al. However the "diffusion barrier" effect by Pt has been demonstrated to be not so effective [25], which can be further supported by the results in Fig. 4 in this study. Although the PtAl coating has a higher DBTT (795 °C [26]) than NiAl (693 °C [24]), no significant through-coating cracks but some ductile deformation shapes were observed in PtAl at 850 °C (Fig. 7(a) and (b)). Addition of Pt prevents the conversion of β to γ' according to the analysing results in section 3.1, which is further demonstrated by the absence of γ' in OZ (Fig. 7(b)). This is probably the reason for the ductile behavior of the OZ in PtAl at 850 °C, different from the brittle behavior of

NiAl (Fig. 6(a) and (b)). Due to the difference of mechanical properties between two characteristic zones, e.g. OZ and IDZ or coating and substrate, some voids/cracks formed at their interface during the creep process at both temperatures (Fig. 7(b) and (c)) but more significant at 950 °C. Toshio [24] also observed such voids in SRZ in PtAl coatings under creep stress. Since the through-coating crack was not formed in PtAl, the "L"-shape crack near the coating part was not observed in this sample type. Either being easily plasticized or producing voids/cracks the coating part lost the ability to carry load during the creep process.

3.2.4. NiAl-PtAl

Comparison of the coating behavior of NiAl in NiAl-PtAl (Fig. 8(a)) with that in NiAl-NiAl (Fig. 6) shows no significant difference at 850 °C. The NiAl can be considered to be ductile at 950 °C since NiAl always shows plastic deformation along the whole cross section of the sample with a few cracks only observed near fracture surface (Fig. 8(b)). The behavior of PtAl looks similar as in PtAl-PtAl type samples at two temperatures: i.e. to be ductile but also to induce cracks beneath the coating or inside of coating.

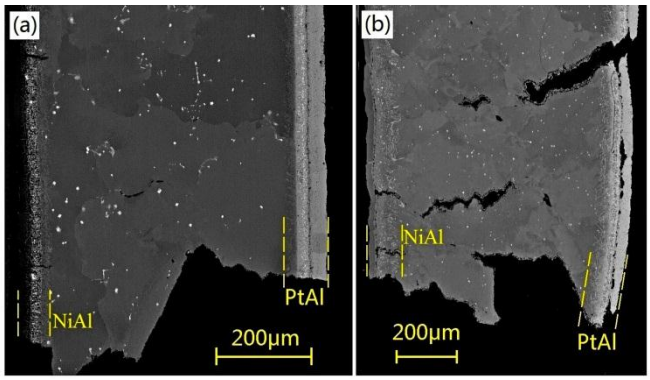

Figure 8. Fractured NiAl-PtAl sample of morphology near fracture surface for (a) 850 °C and (b) 950 °C.

3.3. Summary of creep fracture mechanism

Based on the experimental observations, the crack initiation and propagation mechanisms by which the coating affects the creep fracture behavior are proposed in Fig. 9. For the polycrystalline superalloy grain-boundary separation is always the failure mode in the substrate at 850 °C and 950 °C no matter that the crack initiates from the coating or the substrate. The grain-boundary carbides are beneficial for creep resistance. Due to formation of γ' along grain boundary in outer zone (OZ) at 850 °C NiAl coating can induce active through-coating cracks, which may further penetrate into the substrate along the nearest grain boundary beneath the coating. The γ' in OZ is somewhat restricted in NiAl at 950 °C and in PtAl at both 850 °C and 950 °C, which promotes ductile deformation occurring in the coatings. Even though, PtAl promotes the formation of the voids/cracks either beneath the coating or from inside of coating, caused by the difference of mechanical properties between different characteristic zones. The formed voids/cracks are more active to cause the sample failure at higher temperature.

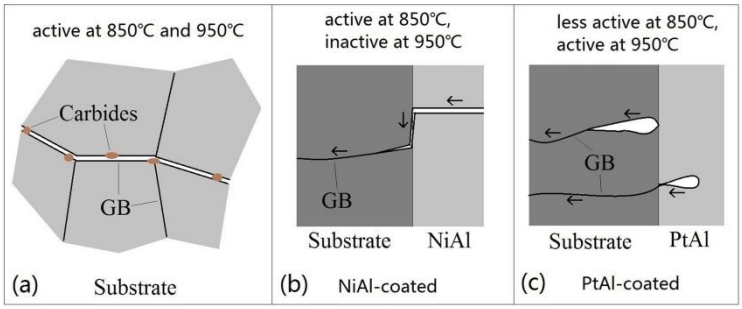

Figure 9. Summary for the crack initiation and propagation mechanism (a) in substrate and by coating's effect of (b) NiAl and (c) PtAl. (GB: grain boundary; Loading direction is vertical; small arrows show the cracking direction)

By using the Larson-Miller approach the creep results in Fig. 2 can be transferred as new ones presented in Fig. 10(a); the plot shows a somewhat negative effect of the coatings lowering the capacity to carry creep stress. Non-loading carrying by coating part above its DBTT was suggested according to some investigations [27]. Being encouraged by the analyses above the applied mechanical load in the creep sample is considered to be mainly carried by the substrate. After recalculating the creep stress by assuming the coating as load-free and excluding the final *effective coating thickness* (*ECT* in Fig. 4) from the total sample thickness, similar performance of coated and uncoated samples is achieved in Larson-Miller diagram (Fig. 10(b)).

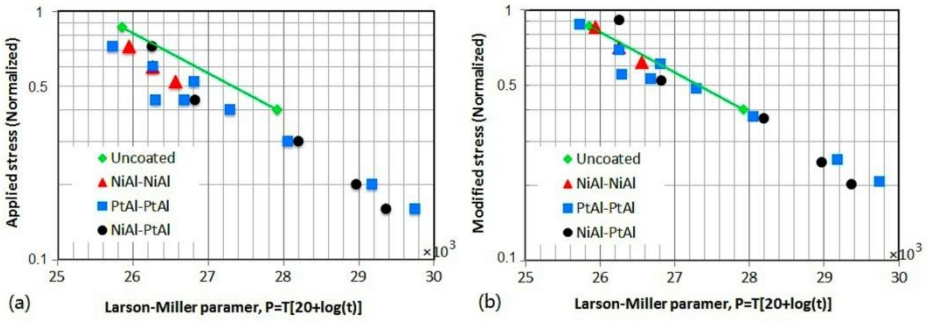

Figure 10. Creep stress (in log-scale and normalized) vs. Larson-Miller parameter (a) before and (b) after stress being modified.

4. Conclusions

In this study the effect of NiAl and PtAl diffusion coatings on the creep fracture mechanism of Ni-based polycrystalline superalloy IN792 is investigated at two temperatures, 850 °C and 950 °C. The following conclusions can be made from this study.

1) The microstructural development of the coating depends on the elemental diffusion during the creep process. The inward diffusion of Al controls the coating thickening rate which seems to be independent of the diffusion coating type.

2) Grain-boundary detachment, which is strengthened by carbides, is the basic cracking mode of the substrate in all samples whether the crack initiated from the coating or the substrate.

3) The diffusion coatings become easily-deformed or induce cracks dependent on coating type and temperature. NiAl is easily deformed at 950 °C but introduces through-coating cracks at 850 °C. PtAl induces voids/cracks in or beneath the coating at both creep temperatures. Those crack initiation modes by PtAl becomes more active when increasing temperature.

4) Based on the results from microstructure analysing, the creep stress of the sample is recalculated by taking the final coating part loading-free. By such stress modification the creep test results of the coated samples are similar with those of the uncoated samples presented in the Larson-Miller diagram. It can be concluded that the applied diffusion coating has a minor influence on the overall creep behavior of the superalloy, but just consuming the effective cross section of the superalloy to carry the creep load.

Acknowledgements

The Siemens Industrial Turbomachinery AB (Finspang, Sweden) is greatly acknowledged for its financial support and supply of materials in this research. The Swedish Energy Agency and GKN Aerospace Engine Systems are also acknowledged for their financial support.

References

[1] R.C. Reed, The Superalloys Fundamentals and Applications, Cambridge, New York, 2006.
[2] J.R. Nicholls, Designing oxidation-resistant coatings, JOM-J. Min. Met. Mat. S. 52 (2000) 28-35.
[3] S. Osgerby, B.F. Dyson, Modelling creep properties of coated superalloys in air and aggressive environments, Mater. Sci. Eng.: A. 120–121, Part 2 (1989) 645-650.
[4] H.J. Kolkman, Creep, Fatigue and Their Interaction in Coated and Uncoated Rene 80, Mater. Sci. Eng. 89 (1987) 81-91.
[5] R.R. Unocic, G.B. Viswanathan, P.M. Sarosi, S. Karthikeyan, J. Li, M.J. Mills, Mechanisms of creep deformation in polycrystalline Ni-base disk superalloys, Mater. Sci. Eng.: A. 483–484 (2008) 25-32.
[6] M.G. Hebsur, R.V. Miner, Stress Rupture and Creep Behavior of a Low Pressure Plasma-Sprayed NiCoCrAlY Coating Alloy in Air and Vacuum, Thin Solid Films. 147 (1987) 143-152.
[7] Y. Itoh, M. Saitoh, Y. Ishiwata, Influence of high-temperature protective coatings on the mechanical properties of nickel-based superalloys, J. of Mater. Sci. (UK). 34 (1999) 3957-3966.
[8] A. Sato, Y. Aoki, M. Arai, H. Harada, Effect of Aluminide Coating on Creep Properties of Ni-Base Single Crystal Superalloys, Journal of the Japan Institute of Metals. 71 (2007) 320-325.
[9] J. Angenete, K. Stiller, A comparative study of two inward grown Pt modified Al diffusion coatings on a single crystal Ni base superalloy, Mater. Sci. Eng. , A. 316 (2001) 182-194.
[10] J. Angenete, K. Stiller, Comparison of inward and outward grown Pt modified aluminide diffusion coatings on a Ni based single crystal superalloy, Surf. Coat. Technol. 150 (2002) 107-118.
[11] N. Vialas, D. Monceau, Effect of Pt and Al content on the long-term, high temperature oxidation behavior and interdiffusion of a Pt-modified aluminide coating deposited on Ni-base superalloys, Surf. Coat. Technol. 201 (2006) 3846-3851.
[12] K. Yuan, R.L. Peng, X.H. Li, L. Johansson, S. Johansson, Y.D. Wang, Analysis on

microstructural evolution of PtAl diffusion coating on Ni-based superalloy influenced by creep process, The 4th Conference on the Integrity of High Temperature Welds & 9th International Conference on Creep and Fatigue. (2012).
[13] Z. Hashin, S. Shtrikman, A Variational Approach to the Theory of the Effective Magnetic Permeability of Multiphase Materials, J. Appl. Phys. 33 (1962) 3125-3131.
[14] J. Agren, Numerical Treatment of Diffusional Reactions in Multicomponent Alloys, J. Phys. Chem. Solids. 43 (1982) 385-391.
[15] Thermo-Calc Software AB, Thermodynamic and Mobility Databases Overview, (2011).
[16] A. Lasalmonie, J.L. Strudel, Influence of Grain Size on the Mechanical Behaviour of Some High Strength Materials, J. Mater. Sci. 21 (1986) 1837-1852.
[17] F.T. Furillo, J.M. Davidson, J.K. Tien, L.A. Jackman, The Effects of Grain Boundary Carbides on the Creep and Back Stress of a Nickel--Base Superalloy, Mater.Sci.Eng. 39 (1979) 267-273.
[18] Q.Z. Chen, N. Jones, D.M. Knowles, The microstructures of base/modified RR2072 SX superalloys and their effects on creep properties at elevated temperatures, Acta Mater. (USA). 50 (2002) 1095-1112.
[19] Q.Z. Chen, C.N. Jones, D.M. Knowles, The grain boundary microstructures of the base and modified RR 2072 bicrystal superalloys and their effects on the creep properties, Mater. Sci. Eng., A. 385 (2004) 402-418.
[20] K. Aning, J.K. Tien, Creep and stress rupture behavior of a wrought nickel-base superalloy in air and vacuum, Mater. Sci. and Eng. 43 (1980) 23-33.
[21] J.M. Larson, Carbide Morphology in P/M IN-792, Metall.Trans.A. 7A (1976) 1497-1502.
[22] R. Lowrie, D.H. Boone, Composite coatings of CoCrAlY plus platinum, Thin Solid Films. 45 (1977) 491-498.
[23] K. Schneider, H.W. Grünling, Mechanical aspects of high temperature coatings, Thin Solid Films. 107 (1983) 395-416.
[24] M. Alam, D. Chatterjee, S. Kamat, V. Jayaram, D. Das, Evaluation of ductile-brittle transition temperature (DBTT) of aluminide bond coats by micro-tensile test method, Mater. Sci. Eng., A: Structural Materials: Properties, Microstructures and Processing. 527 (2010) 7147-7150.
[25] P. Hancock, H.H. Chien, J.R. Nicholls, D.J. Stephenson, In situ measurements of the mechanical properties of aluminide coatings, Surf. and Coat. Technol. 43–44, Part 1 (1990) 359-370.
[26] S. Bose, High Temperature Coatings, Butterworth-Heinemann, Oxford, 2007.
[27] T. Narita, A View of Compatible Heat-Resistant Alloy and Coating Systems at High-Temperatures, Proceedings of the International Workshop On Advanced Material For New and Renewable Energy. (2009) 63-67.
[28] T.K. Chaki, A.K. Singh, K. Sadananda, Effects of CoCrAlY coating on microstructural stability and creep behavior of a nickel-base superalloy, Thin Solid Films. 168 (1989) 207-220.